Examining and extending the concept of machine acceleration used in modelling the bubble-particle detachment in flotation

Duc Ngo-Cong[a,*] and Anh V. Nguyen [b,*]

[a] University of Southern Queensland, Institute for Advanced Engineering and Space Sciences, Toowoomba, QLD 4350, Australia

[b] School of Chemical Engineering, The University of Queensland, Brisbane, QLD 4072, Australia

ABSTRACT

The bubble-particle (BP) detachment is a significant factor in controlling the recovery of coarse particles in mechanical flotation cells. It has been quantified by balancing the restoring force of surface tension and the centrifugal force exerted on the particle-bubble aggregate by the turbulent flow field using a "machine acceleration". The concept of machine acceleration is useful because it links the mean energy dissipation rate of turbulence with the condition of the BP detachment. Here we further examine the concept of machine acceleration by applying the theory of isotropic turbulence. We confirm the known results of the first approximation for the inertial subrange. We also show that the turbulence acceleration has two principal components, i.e., the longitudinal and transverse components measured relatively to the BP centre-line. Significantly, the longitudinal component corresponds to the centrifugal force of turbulence against the restoring force of surface tension. The transverse component can be significant to quantifying the BP detachment if the turbulence shear is strong. We also extend the theory to cover the full range of isotropic turbulence, from the viscous to inertial subranges. Our estimation of the transition from the viscous to inertial subrange shows that the viscous effect can critically affect the BP detachment. Finally, our assessment of the contributions of the longitudinal and transverse components to the machine acceleration reveals the importance of the transverse component which can lead to a rather poor approximation for the machine acceleration as currently used. This paper shows that the effect of turbulence on the BP detachment should be better quantified using both the longitudinal and transverse components of turbulence acceleration rather than their modulus as the first approximation being termed the machine acceleration.

Keywords: machine acceleration; turbulence; bubble-particle detachment; flotation theory

*Correspondence: duc.ngo@usq.edu.au (Duc Ngo-Cong), anh.nguyen@eng.uq.edu.au (Anh V. Nguyen)

1. INTRODUCTION

In the operation of mechanical flotation cells, the ore is ground to a given degree of a fineness sufficient to liberate valuable particles from gangue particles (Jameson, 2010; Nguyen and Schulze, 2004; Wang et al., 2016b). The rate of recovery of minerals from flotation pulps reduces with increasing particle size due to the detachment of coarse particles from bubbles in the region of high rate of energy dissipation (Goel and Jameson, 2012; Schulze, 1977, 1982). It is highly desired to establish a suitable particle size to maximise the flotation recovery and minimise the unnecessary consumption of energy spent on overgrinding. However, this task of optimisation remains unsolved since our understanding of the BP detachment is still limited due to the complex (multiphase and multiscale) dynamics of turbulence involved in flotation.

During the past decades, many researchers have investigated the bubble-particle detachment phenomenon in flotation both experimentally and theoretically. It is established that except for the region far away from the impeller, the turbulent flow is isotropic and can be described by the Kolmogorov theory of isotropic turbulence. Schulze (Schulze, 1977, 1982) developed a model based on the isotropic turbulence theory to quantify the BP detachment. The key assumption of the theory is that the bubble-particle aggregate is trapped inside a rotating eddy of the scale of isotropic turbulence. In his theory, Schulze introduced and used the Bond number (Bo) which is defined by the ratio of the centrifugal to surface tension force. The particle detaches from the bubble if the centrifugal force on the particle exceeds the surface tension force, i.e., $Bo>1$. The centrifugal force is a known detaching force and is a function of the machine acceleration which is denoted by b_m. Schulze's theory of detachment has been followed by many researchers (Goel and Jameson, 2012; Nguyen and Schulze, 2004; Wang et al., 2016a, 2017). In Schulze's theory (Schulze, 1977, 1982), it is assumed that the radius of rotation is equal to the bubble diameter. Recently, it is considered by Jameson et al. (Goel and Jameson, 2012; Jameson et al., 2007) that the diameter of rotation is equal to the diameter of the bubble. Nothing is wrong with these two hypotheses since the first hypothesis is true if the centre of the eddy rotation is at the bubble surface while the second one is valid if the rotation is centred at the bubble centre. Unfortunately, direct experiments to provide data for validating the assumptions are limited. Based on their experimental results, Goel and Jameson (2012) found that the detachment occurs over a range of their modified Bond numbers (Bo_m), even

when the Bond numbers are quite small ($Bo_m = 0.45, Bo = 0.4$). Wang et al. (2016a) conducted a novel experiment with a BP aggregate introducing into a cavity flow to study the BP detachment in a rotating eddy and verify Schulze's theory of detachment (Schulze, 1977, 1982). Their results showed that the averaged centrifugal acceleration is nearly 23 times gravitational acceleration at detachment, i.e. the gravity effect on detachment is negligible compared to the effect of turbulence. The authors also developed a BP detachment model using the computational fluid dynamic (CFD) approach with several turbulence models, neglecting the effect of bubble and particle motion on the surrounding fluid (Wang et al., 2017). In their model, the centrifugal acceleration b_m and the probability of particle detachment P_d are determined as a function of the turbulence vorticity, ω. The particle detachment ($P_d > 1$) occurs in the regions on the top and bottom of the wall cavity near the downstream wall where the vorticity, the shear rate and the energy dissipation rate are high.

In this article, we examine and extend the concept of machine acceleration used to model the BP detachment in flotation. The correlation of bubble and particle accelerations is calculated by using the correlation method in conjunction with the theory of isotropic turbulence. The bubbles and solid particles are represented by the fluid particles at their locations whose motion is governed by the Navier-Stokes equations (NSEs). The bubble-particle acceleration correlation is approximated by the fluid-fluid particle acceleration correlation having two principal components, i.e., the longitudinal and transverse components measured relatively to the BP centre-line. Their modulus for the inertial subrange is the known machine acceleration. Then we investigate the influence of bubble and particle sizes, and dissipation rate of turbulence energy on the machine acceleration and the longitudinal and transverse components of the BP acceleration correlation. We also extend the theory to cover the full range of isotropic turbulence, from the viscous to inertial subranges, and compare the obtained results with those for the inertial subrange.

2. CORRELATION OF FLUCTUATING ACCELERATION OF TWO LIQUID PARTICLES

As the first approximation, the bubbles and solid particles are represented by the fluid particles at their locations whose motion is governed by NSEs with the Lagrangian frame of reference and is described as follows:

$$a_i = \frac{dV_i}{dt} = -\frac{1}{\rho}\frac{\partial p}{\partial x_i} + \nu \Delta V_i \tag{1}$$

Applying the Reynolds decomposition where the instantaneous quantities are decomposed into their time-averaged and fluctuating components (i.e. $V_i = \overline{V}_i + V_i^{'}$, $a_i = \overline{a}_i + a_i^{'}$, and $p = \overline{p} + p^{'}$), Eq. (1) gives

$$a_i^{'} = \frac{dV_i^{'}}{dt} = -\frac{1}{\rho}\frac{\partial p^{'}}{\partial x_i} + \nu \Delta V_i^{'} \tag{2}$$

Hereafter, we only deal with the fluctuating terms (i.e., fluctuating velocity, acceleration and pressure) and the prime denoting fluctuations is neglected for simplicity. Therefore, Eq. (2) is rewritten as follows:

$$a_i = \frac{dV_i}{dt} = -\frac{1}{\rho}\frac{\partial p}{\partial x_i} + \nu \Delta V_i, \tag{3}$$

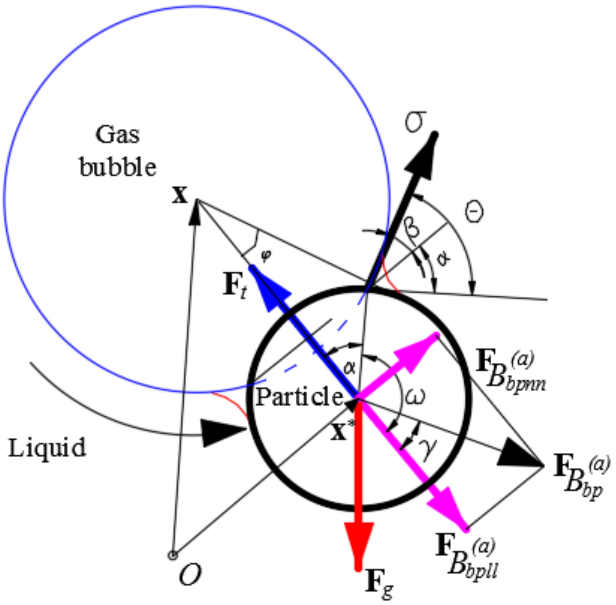

Figure 1. A bubble-particle detachment model (not to scale), designed relative to an origin *O*.

The correlation of the fluctuating acceleration of fluid particles at positions $\mathbf{x}$ (bubble position) and $\mathbf{x}^*$ (particle position) is determined by

$$B_{ij}^{(a)}(r)=\overline{a_i(\mathbf{x})a_j(\mathbf{x}^*)}=\overline{a_i a_j^*}=\overline{\left(-\frac{1}{\rho}\frac{\partial p}{\partial x_i}+\nu\Delta V_i\right)\left(-\frac{1}{\rho}\frac{\partial p^*}{\partial x_j^*}+\nu\Delta^* V_j^*\right)} \tag{4}$$

where $r=\left|\mathbf{x}^*-\mathbf{x}\right|$. Since the random scalar field p and the random solenoidal vector field V do not correlate with each other (Panchev and Haar, 1971), we obtain $\overline{\frac{\partial p}{\partial x_i}\Delta^* V_j^*}=0$ and $\overline{\Delta V_i\frac{\partial p^*}{\partial x_j^*}}=0$. Eq. (4) can be expanded, giving:

$$B_{ij}^{(a)}(r)=\frac{1}{\rho^2}\overline{\frac{\partial p}{\partial x_i}\frac{\partial p^*}{\partial x_j^*}}+\nu^2\Delta\Delta^*\overline{V_i V_j^*}=\frac{1}{\rho^2}\frac{\partial^2 B^{(p)}(r)}{\partial x_i\partial x_j^*}+\nu^2 D_3^2 B_{ij}^{(V)}(r) \tag{5}$$

Two terms on the right hand side of Eq. (5) are the correlations of acceleration due to the pressure and velocity fields, respectively. They are defined by the following equations:

$$B_{ij}^{\left(a^{(p)}\right)}(r)=\frac{1}{\rho^2}\frac{\partial^2}{\partial x_i\partial x_j^*}B^{(p)}(r) \tag{6}$$

$$B_{ij}^{\left(a^{(V)}\right)}(r)=\nu^2 D_3^2 B_{ij}^{(V)}(r) \tag{7}$$

The transverse and longitudinal components of $B_{ij}^{\left(a^{(p)}\right)}(r)$ and $B_{ij}^{\left(a^{(V)}\right)}(r)$ are obtained from Eqs. (6) and (7). The detailed derivations can be found in the Appendix. The results are given as follows:

$$B_{nn}^{\left(a^{(p)}\right)}(r)=-\frac{1}{\rho^2 r}\frac{\partial B^{(p)}}{\partial r} \tag{8}$$

$$B_{ll}^{\left(a^{(p)}\right)}(r)=-\frac{1}{\rho^2}\frac{\partial^2 B^{(p)}}{\partial r^2} \tag{9}$$

$$B_{nn}^{\left(a^{(V)}\right)}=\nu^2\left(\frac{24}{r}\frac{\partial f}{\partial r}+36\frac{\partial^2 f}{\partial r^2}+8r\frac{\partial^3 f}{\partial r^3}+f_n\right) \tag{10}$$

$$B_{ll}^{\left(a^{(V)}\right)} = \nu^2 \left(\frac{24}{r}\frac{\partial f}{\partial r} + 36\frac{\partial^2 f}{\partial r^2} + 12r\frac{\partial^3 f}{\partial r^3} + r^2\frac{\partial^4 f}{\partial r^4} + f_n \right) \tag{11}$$

where the functions f and f_n are defined by

$$f = \frac{B_{ll}^{(V)} - B_{nn}^{(V)}}{r^2} \tag{12}$$

$$f_n = D_3^2\left(B_{nn}^{(V)}\right) \tag{13}$$

The structure function of pressure fluctuations $D^{(p)}(r)$ in Eq. (13) can be determined from the theory of isotropic turbulence (Panchev and Haar, 1971) and can be described as follows:

$$D^{(p)}(r) = \rho^2 \left[\int_0^r \zeta \left(\frac{\partial D_{ll}^{(V)}}{\partial \zeta} \right)^2 d\zeta + \int_r^\infty \zeta^{-1} \left(\frac{\partial D_{ll}^{(V)}}{\partial \zeta} \right)^2 d\zeta \right] \tag{14}$$

It is noted that Eq. (14) is applicable for the entire range of distance r between the particles.

If the structure function of pressure fluctuations $D^{(p)}(r)$ is known, then the correlation function of pressure fluctuations can then be determined (Panchev and Haar, 1971) and gives

$$B^{(p)}(r) = B^{(p)}(0) - \frac{1}{2}D^{(p)}(r) \tag{15}$$

where $B^{(p)}(0)$ is a constant. The following Sections focus on modelling the machine acceleration.

2.1 General prediction of the machine acceleration, $b_m^{(a)}$

The potential vector field $a_i^{(p)} = -(1/\rho)\partial p/\partial x_i$ and the solenoidal vector field $a_i^{(V)} = \nu\Delta V$ are stochastically homogeneous and isotropic, and hence they are stochastically uncorrelated. Therefore, we have

$$B_{ll}^{(a)} = B_{ll}^{\left(a^{(p)}\right)} + B_{ll}^{\left(a^{(V)}\right)} \tag{16}$$

$$B_{nn}^{(a)} = B_{nn}^{\left(a^{(p)}\right)} + B_{nn}^{\left(a^{(V)}\right)} \tag{17}$$

where $\left(B_{nn}^{\left(a^{(p)}\right)}, B_{ll}^{\left(a^{(p)}\right)}\right)$ and $\left(B_{nn}^{\left(a^{(V)}\right)}, B_{ll}^{\left(a^{(V)}\right)}\right)$ are determined by Eqs. (8)-(11). The magnitude of the correlation of the fluctuating accelerations is calculated as follows:

$$b_m^{(a)} = \sqrt{\left|B_{ll}^{(a)}\right| + \left|B_{nn}^{(a)}\right|} \tag{18}$$

where the vertical bars denote the modulus (i.e., the magnitude) of vector-like variables – in the case of numbers they describe the absolute values. Note that the force associated with the correlation of the fluctuating accelerations ($\mathbf{F}_{B_{bp}^{(a)}}$) is a detaching force, causing the particle detachment from the bubble surface. This force has two principal components, i.e., the longitudinal and transverse components measured relatively to the BP centre-line, i.e., $\mathbf{F}_{B_{bpll}^{(a)}}$ and $\mathbf{F}_{B_{bpnn}^{(a)}}$, as shown in **Figure 1**. In the present study, the bubble and particle are represented by two fluid particles as per the first principle employed in the current modelling of BP detachment interaction. Thus, $\mathbf{F}_{B_{bpll}^{(a)}}$ and $\mathbf{F}_{B_{bpnn}^{(a)}}$ are the functions of $B_{ll}^{(a)}$ and $B_{nn}^{(a)}$, respectively.

The angle between the total force $\mathbf{F}_{B_{bp}^{(a)}}$ and the BP centre-line can also be calculated as shown by Eq. (19).

$$\gamma = \arctan\left(\frac{F_{B_{bpnn}^{(a)}}}{F_{B_{bpll}^{(a)}}}\right) = \arctan\sqrt{\left|\frac{B_{nn}^{(a)}}{B_{ll}^{(a)}}\right|} \tag{19}$$

where $F_{B_{bpnn}^{(a)}} = m_p\sqrt{\left|B_{nn}^{(a)}\right|}$ and $F_{B_{bpll}^{(a)}} = m_p\sqrt{\left|B_{ll}^{(a)}\right|}$.

2.2 Modelling of $b_m^{(a)}$ in the inertial subrange

2.2.1 Determination of $D_{ll}^{(V)}, D_{nn}^{(V)}, B_{ll}^{(V)}, B_{nn}^{(V)}$ in the inertial subrange

In the inertial subrange, the second-order longitudinal structure function is given by the following equation (Alipchenkov and Zaichik, 2003; Panchev and Haar, 1971):

$$D_{ll}^{(V)}(r) = C\varepsilon^{2/3} r^{2/3} \tag{20}$$

where $C \approx 2.0$ is a numerical constant. Substituting Eq. (20) into Eq. (14) yields

$$D^{(p)}(r) = \rho^2 C^2 (\varepsilon r)^{4/3} = \rho^2 \left(D_{ll}^{(V)}\right)^2 \tag{21}$$

Inserting Eq. (21) into Eq. (15) gives

$$B^{(p)}(r) = B^{(p)}(0) - \frac{1}{2}\rho^2 C^2 \varepsilon^{4/3} r^{4/3} \tag{22}$$

The longitudinal and transverse components of the velocity correlation $B_{ll}^{(V)}$ and $B_{nn}^{(V)}$ are determined as follows:

$$B_{ll}^{(V)} = B_{ll}^{(V)}(0) - \frac{1}{2} D_{ll}^{(V)}(r), \tag{23}$$

where $B_{ll}^{(V)}(0) = B_{nn}^{(V)}(0) = u_0^2$ are available for the homogeneous and isotropic random velocity field. Therefore, we obtain

$$B_{ll}^{(V)} = u_0^2 - \frac{1}{2} C (\varepsilon r)^{2/3} \quad \therefore \quad \frac{\partial B_{ll}^{(V)}}{\partial r} = -\frac{C}{3} \varepsilon^{2/3} r^{-1/3} \tag{24}$$

$$B_{nn}^{(V)} = B_{ll}^{(V)} + \frac{r}{2} \frac{\partial B_{ll}^{(V)}}{\partial r} = u_0^2 - \frac{2C}{3} \varepsilon^{2/3} r^{2/3} \tag{25}$$

Substituting Eqs. (24) and (25) into Eq. (12) gives

$$f(r) = \frac{1}{6} C \varepsilon^{2/3} r^{-4/3} \tag{26}$$

Substituting Eq. (25) into Eq. (13) also gives

$$f_n = -\frac{80C}{243} \varepsilon^{2/3} r^{-10/3} \tag{27}$$

2.2.2 Determination of $b_m^{(a)}$ in the inertial subrange

Substituting Eq. (22) into Eqs. (8) and (9), the correlation functions $B_{nn}^{(a^{(p)})}(r)$ and $B_{ll}^{(a^{(p)})}(r)$ are obtained as follows:

$$B_{nn}^{(a^{(p)})}(r) = \frac{8}{3} \varepsilon^{4/3} r^{-2/3} \tag{28}$$

$$B_{ll}^{(a^{(p)})}(r) = \frac{8}{9} \varepsilon^{4/3} r^{-2/3} \tag{29}$$

Substituting Eqs. (26) and (27) into Eqs. (10) and (11) yields

$$B_{nn}^{(a^{(V)})} = -\frac{400}{243} \varepsilon^{2/3} \nu^2 r^{-10/3} \tag{30}$$

$$B_{ll}^{(a^{(V)})} = -\frac{40}{81} \varepsilon^{2/3} \nu^2 r^{-10/3} \tag{31}$$

Making use of Eqs. (18), (28), (29), (30), and (31), the magnitude of the correlation of the fluctuating accelerations b_m is obtained as follows:

$$b_m^{(a)} = \sqrt{\left| \frac{8}{9} \varepsilon^{4/3} r^{-2/3} - \frac{40}{81} \varepsilon^{2/3} \nu^2 r^{-10/3} \right| + \left| \frac{8}{3} \varepsilon^{4/3} r^{-2/3} - \frac{400}{243} \varepsilon^{2/3} \nu^2 r^{-10/3} \right|} \tag{32}$$

Neglecting the viscous effect, Eq. (18) reduces to

$$b_m^{\left(a^{(p)}\right)} = \sqrt{\left|B_{ll}^{\left(a^{(p)}\right)}(r)\right| + \left|B_{nn}^{\left(a^{(p)}\right)}(r)\right|} = \sqrt{\frac{8}{9}\varepsilon^{4/3}r^{-2/3} + \frac{8}{3}\varepsilon^{4/3}r^{-2/3}} \approx 1.9\frac{\varepsilon^{2/3}}{r^{1/3}} \tag{33}$$

which is identical to the mean machine acceleration introduced by Schulze (1982).

2.3 Modelling of $b_m^{(a)}$ in the entire range of isotropic turbulence length scale

2.3.1 Determination of $D_{ll}^{(V)}, D_{nn}^{(V)}, B_{ll}^{(V)}, B_{nn}^{(V)}$ in the entire range

A continuous description of the longitudinal structure function of velocity fluctuations for the entire range of distances r can be approximated as follows (Zaichik et al., 2008):

$$D_{ll}^{(V)} = 2u_0^2\left[1-\exp\left(-\frac{\bar{r}}{(15C)^{3/4}}\right)\right]^{4/3}\left(\frac{15^3\bar{r}^4}{15^3\bar{r}^4+\left(2\,\mathrm{Re}_\lambda/C\right)^6}\right)^{1/6} \tag{34}$$

where $\bar{r} = r/\lambda_K$. Upon expanding the terms of Eq. (34), we obtain

$$D_{ll}^{(V)} = 2u_0^2\left[1-\mathrm{e}^{-k_{D1}r}\right]^{4/3}\left(\frac{15^3r^4}{15^3r^4+k_{D2}}\right)^{1/6} \tag{35}$$

The model parameters in Eq. (35) are defined as follows:

$$k_{D1} = \frac{1}{\lambda_K(15C)^{3/4}} \tag{36}$$

$$k_{D2} = \lambda_K^4\left(2\,\mathrm{Re}_\lambda/C\right)^6 \tag{37}$$

Taking the derivative and arranging the results yield

$$\frac{\partial D_{ll}^{(V)}}{\partial r} = 4\sqrt{\frac{5}{3}}u_0^2\,\mathrm{e}^{-k_{D1}r}\left(\frac{1-\mathrm{e}^{-k_{D1}r}}{r}\right)^{1/3}\left(\frac{1}{15^3 r^4 + k_{D2}}\right)^{7/6} \times\left[\left(-1+\mathrm{e}^{k_{D1}r}\right)k_{D2} + 2rk_{D1}\left(15^3 r^4 + k_{D2}\right)\right] \tag{38}$$

For the solenoidal velocity field of water flow, in three-dimensional space, the transverse component of the structure function is calculated from the longitudinal component as follows (Panchev and Haar, 1971):

$$D_{nn}^{(V)} = D_{ll}^{(V)} + \frac{r}{2}\frac{\partial D_{ll}^{(V)}}{\partial r} \tag{39}$$

It is recalled that in Eqs. (36) and (37), $C \approx 2$ and the Reynolds number Re_λ calculated for the Taylor microscale is given by

$$\mathrm{Re}_\lambda = \left(\frac{15u_0^4}{\varepsilon\nu}\right)^{1/2} \tag{40}$$

Substituting Eq. (38) into Eq. (14) and calculating the integrals in Eq. (14) approximately using the trapezoidal method, we get the structure function of pressure fluctuations in the entire range of r. The correlation function of pressure $B^{(p)}(r)$ is then obtained by Eq. (15). The first and second derivatives of the function $B^{(p)}(r)$ are approximately calculated using the central-finite difference schemes. In addition, the longitudinal and transverse components of the velocity correlation ($B_{ll}^{(V)}$ and $B_{nn}^{(V)}$) for the entire range are determined as follows:

$$B_{ll}^{(V)} = u_0^2 - u_0^2\left[1-\mathrm{e}^{-k_{D1}r}\right]^{4/3}\left(\frac{15^3 r^4}{15^3 r^4 + k_{D2}}\right)^{1/6} \tag{41}$$

Finally, we obtain the following useful predictions for calculating the machine acceleration:

$$\frac{\partial B_{ll}^{(V)}}{\partial r} = -u_0^2 \left\{ \begin{array}{l} \frac{4}{3} k_{D1} \left[1 - \mathrm{e}^{-k_{D1} r}\right]^{1/3} \mathrm{e}^{-k_{D1} r} \left(\frac{15^3 r^4}{15^3 r^4 + k_{D2}} \right)^{1/6} + \\ \left[1 - \mathrm{e}^{-k_{D1} r}\right]^{4/3} 2250 \left(\frac{15^3 r^4}{15^3 r^4 + k_{D2}} \right)^{-5/6} \left[\frac{k_{D2} r^3}{\left(15^3 r^4 + k_{D2}\right)^2} \right] \end{array} \right\} \tag{42}$$

$$B_{nn}^{(V)} = B_{ll}^{(V)} + \frac{r}{2} B_{ll}^{(V)'} \tag{43}$$

2.3.2 Determination of $b_m^{(a)}$ in the entire range

The value of $b_m^{(a)}$ for the entire range of r can be numerically calculated employing Eqs. (8)-(18). The numerical results are presented and discussed below.

3. RESULTS AND DISCUSSION

3.1 Verification of the numerical model using the results for the inertial subrange

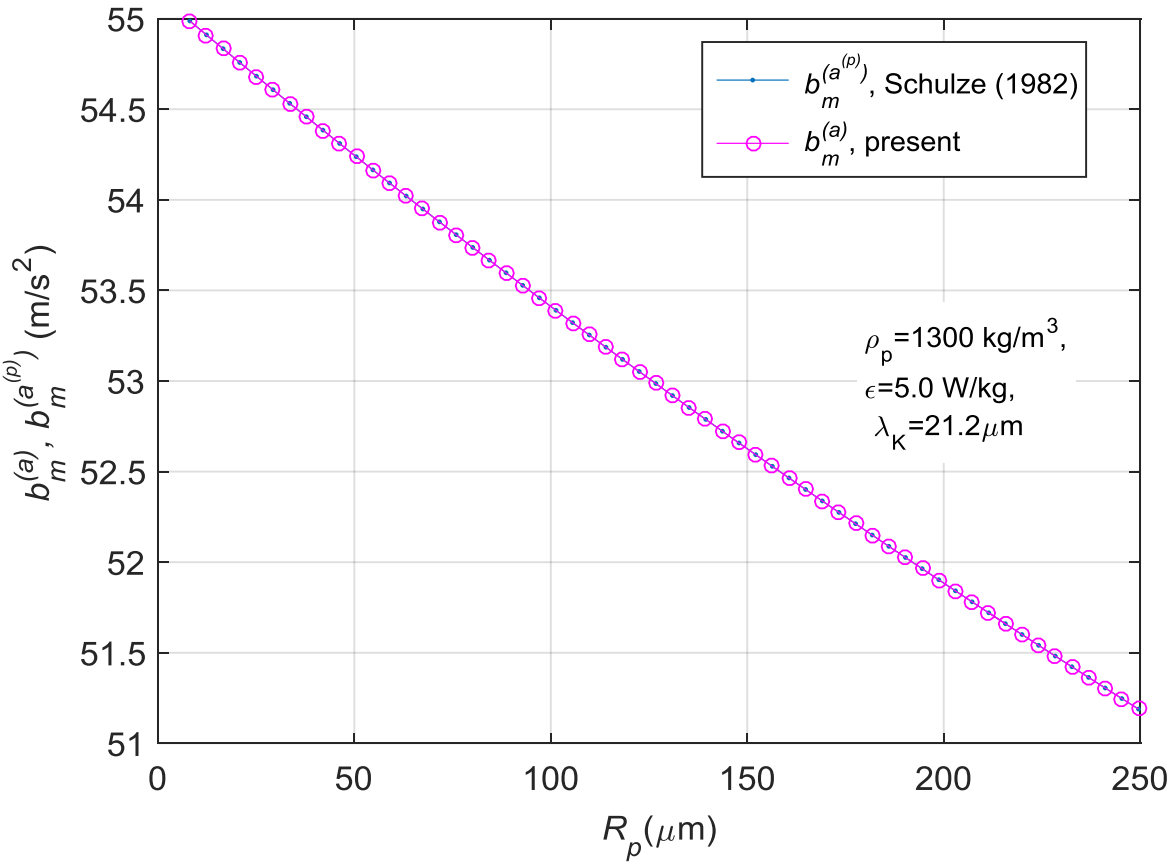

Figure 2. Comparison of the mean machine acceleration b_m w.r.t. R_p between Schulze's model and Model 1, for $R_b = 1\,\text{mm}$ and $\varepsilon = 5.0\ \text{W/kg}$.

As mentioned above, our present model takes into account both the pressure and viscous effects while Schulze (1982)'s model neglects the viscous effect. The results obtained by both the models for the inertial subrange are indistinguishable as shown in **Figure 2**, indicating that the machine acceleration mainly depends on the local gradient of pressure, not on the viscous force.

Since the structure function for the full range of isotropic turbulence (Eq. (35)) is much more complicated than that for the inertial subrange as described by Eq. (20), it is very difficult to obtain the analytic expression of the machine acceleration $b_m^{(a)}$ for the full range. Therefore, we use a numerical approach based on the finite difference method for approximating the derivatives in the process of calculating $b_m^{(a)}$ and the trapezoidal method for the integrals.

Firstly, we verify our numerical approach through the solution of $b_m^{\left(a^{(p)}\right)}$ for the inertial subrange. The obtained numerical result is compared with the analytic solution of $b_m^{\left(a^{(p)}\right)}$ given by Eq. (33). We determine the structure function of pressure fluctuations $D^{(p)}(r)$ by Eq. (14) where the integrals are approximated using the trapezoidal method. Since the upper limit of the second integral (called $\zeta_{\max}$) is infinite, we need to choose $\zeta_{\max}$ large enough to obtain the converged result of the integrals. The dependence of the solution on $\zeta_{\max}$ is investigated below. The correlation function of pressure $B^{(p)}(r)$ is then obtained by Eq. (15). The first and second derivatives of the function $B^{(p)}(r)$ ($\partial B^{(p)}/\partial r$ and $\partial^2 B^{(p)}/\partial r^2$) are approximately calculated using the central-finite difference schemes. Since the values of $\partial B^{(p)}/\partial r$ and $\partial^2 B^{(p)}/\partial r^2$ are determined numerically, we need to conduct the grid convergence study of $\partial B^{(p)}/\partial r$ and $\partial^2 B^{(p)}/\partial r^2$ to determine a grid size Δr which is fine enough to get accurate results.

The relative error norm $Ne(u)$ is calculated as follows:

$$Ne(u) = \sqrt{\frac{\sum_{i=1}^{N}\left(u^{(i)} - u_a^{(i)}\right)^2}{\sum_{i=1}^{N}\left(u_a^{(i)}\right)^2}} \tag{44}$$

where the subscript a represents the analytic solution; and N the total number of grid points in the computational domain. If the numerical solution is convergent, the relative error norm Ne reduces with respect to the grid refinement and the increase of $\zeta_{\max}$.

Figure 3 shows the dependence of the results of $b_m^{(a^{(p)})}$, $D^{(p)}(r)$, $\partial B^{(p)}/\partial r$ and $\partial^2 B^{(p)}/\partial r^2$ on the values of $\zeta_{\max}$ and Δr. As expected, the larger $\zeta_{\max}$ and the smaller Δr, the more accurate the solution is. The approximate and analytic results of $b_m^{(a^{(p)})}$ as well as $D^{(p)}(r)$, $\partial B^{(p)}/\partial r$ and $\partial^2 B^{(p)}/\partial r^2$ are in good agreement as shown in **Figure 4** for $\zeta_{\max}=1.0\,m, \Delta r=\lambda_K/5=4.2\mu m$. Therefore, we choose $\zeta_{\max}=1.0\,m, \Delta r=\lambda_K/5=4.2\mu m$ for the following numerical calculations.

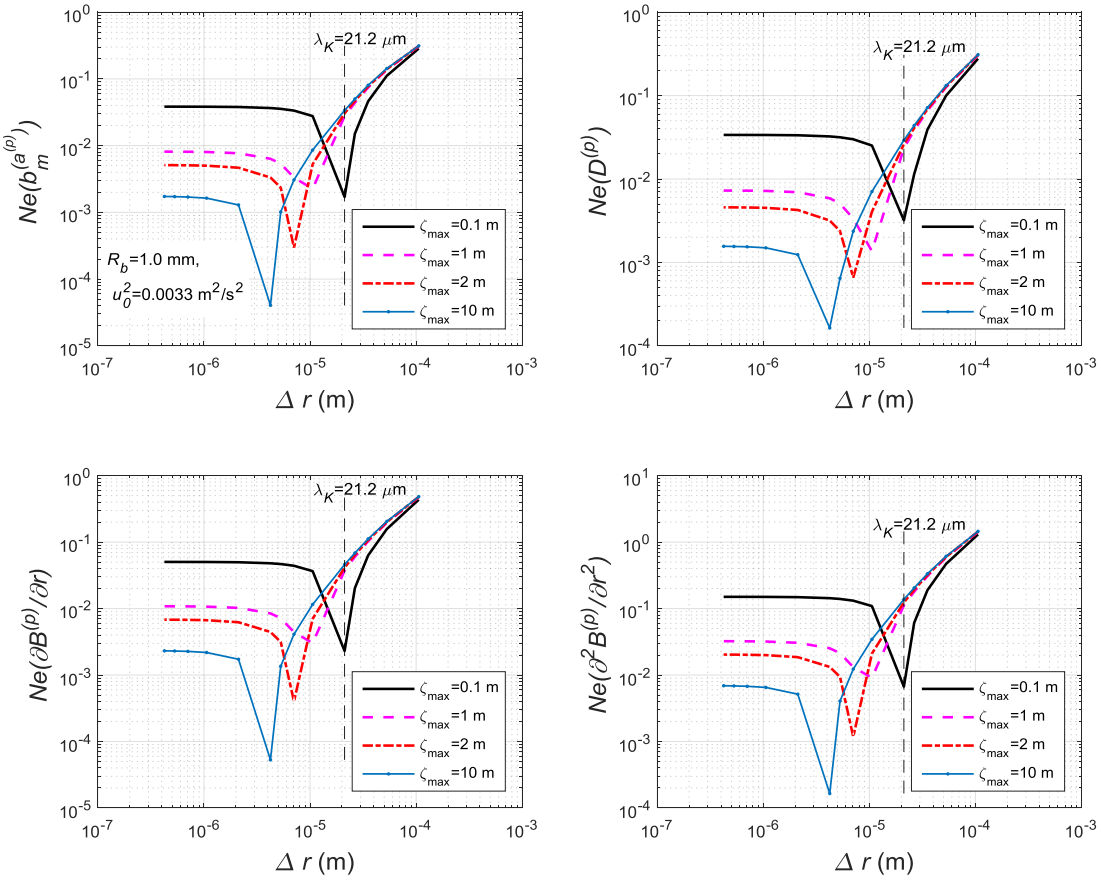

Figure 3. The inertial subrange case: grid convergence study of $b_m^{(a^{(p)})}$, $D^{(p)}(r)$, $\partial B^{(p)}/\partial r$ and $\partial^2 B^{(p)}/\partial r^2$ versus the grid size Δr for different values of $\zeta_{\max}=\{0.1, 1.0, 2.0, 10.0\}\,m$.

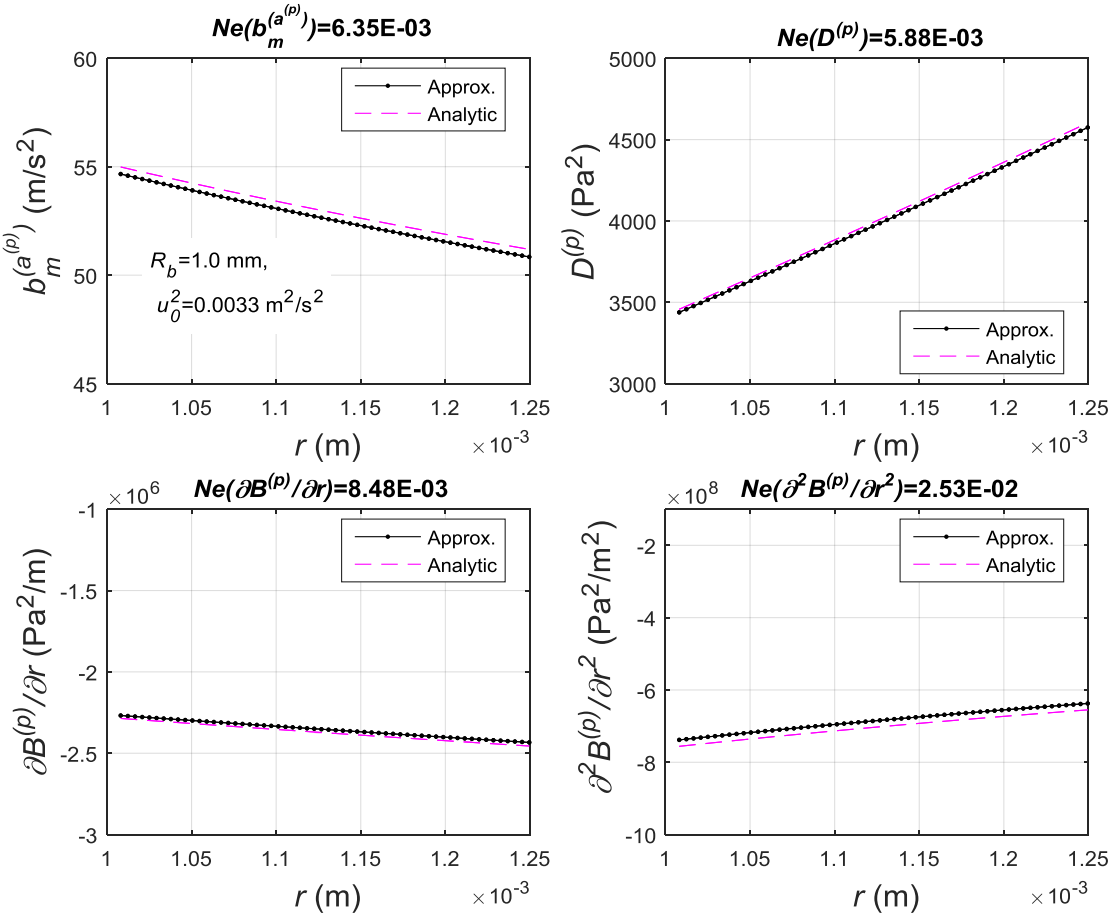

Figure 4. The inertial subrange case: comparison of $b_m^{(a^{(p)})}$, $D^{(p)}(r)$, $\partial B^{(p)}/\partial r$ and $\partial^2 B^{(p)}/\partial r^2$ profiles between the approximate and analytic results for $\zeta_{\max}$=1.0 m, $\Delta r = \lambda_K/5$=4.2μm.

3.2 Comparison of results between the inertial subrange and the entire range of isotropic turbulence

Figure 5 presents the comparison of results between the inertial subrange $D_{ll}^{(V)}(r)$ profile (Eq. (20)) and the entire range $D_{ll}^{(V)}(r)$ profile (Eq. (35)) for $\zeta_{\max}$=1.0 m, $\Delta r = \lambda_K/5$=4.2μm and u_0^2=0.0033 m^2/s^2. Note that the former profile is just valid in the inertial subrange ($\lambda_K \ll r \ll \Lambda$, Λ is the macro-turbulence length scale (Nguyen et al., 2016)). Here, the bubble size is R_b=1 mm=47.2λ_K. The entire range $D_{ll}^{(V)}(r)$ profile is suitable for a wide range of turbulent length scales. It can be seen in **Figure 5** that the results of $b_m^{(a^{(p)})}$ and $b_m^{(a)}$ associated with the entire range profile are much smaller than those associated with the inertial range profile. The corresponding

results for $u_0^2=1\,\mathrm{m}^2/\mathrm{s}^2$ are presented in **Figure 6** showing that the results of $b_m^{\left(a^{(p)}\right)}$ and $b_m^{(a)}$ associated with the entire range profile are also smaller than those associated with the inertial range profile. It appears that the results of the present model ($b_m^{(a)}$) and those of Schulze (1982) ($b_m^{\left(a^{(p)}\right)}$) almost coincide for both the cases of inertial subrange and entire range.

For the entire range, the magnitude of $B_{nn}^{(a)}$ is smaller than that of $B_{ll}^{(a)}$ thus $\gamma^{(a)}<45^\circ$ for $u_0^2=0.0033\,\mathrm{m}^2/\mathrm{s}^2$ (**Figure 7**) while the magnitude of $B_{nn}^{(a)}$ is larger than that of $B_{ll}^{(a)}$ thus $\gamma^{(a)}>45^\circ$ for $u_0^2=1\,\mathrm{m}^2/\mathrm{s}^2$ (**Figure 8**). This indicates that the transverse component of turbulence acceleration $\left(B_{nn}^{(a)}\right)$ becomes more important as the turbulence intensity (u_0^2) is stronger. The influence of u_0^2 on the turbulence acceleration is further investigated in the following section.

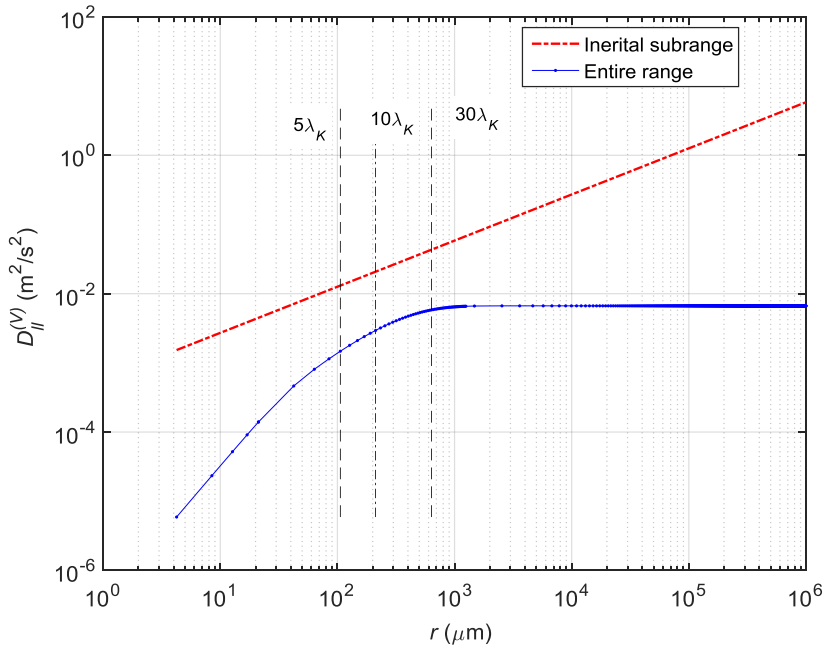

(a)

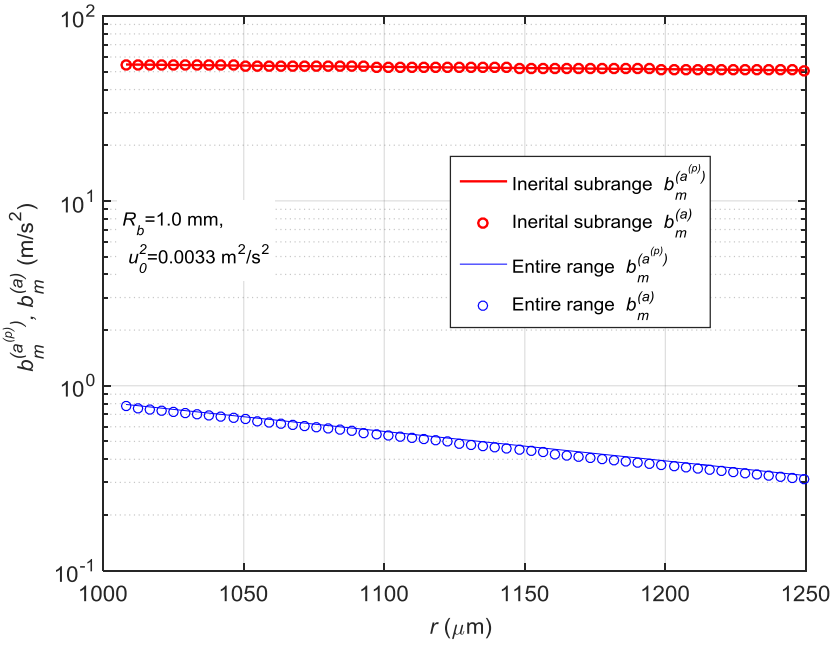

(b)

Figure 5. Comparison of $b_m^{(a)}$ and $b_m^{(a^{(p)})}$ results between the inertial subrange and the entire range for $\zeta_{\max}$=1.0 m, $\Delta r = \lambda_K / 5$=4.2μm and u_0^2=0.0033 m^2/s^2.

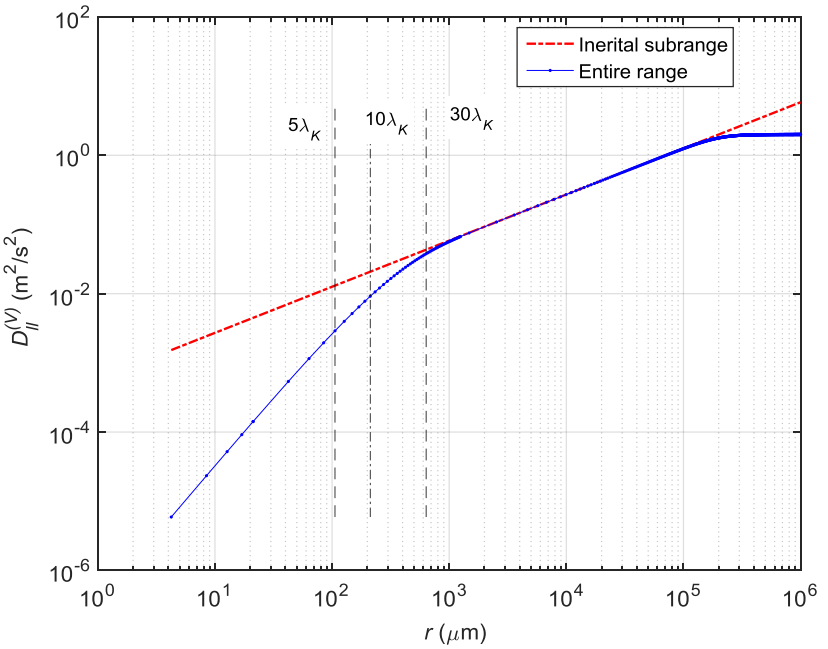

(a)

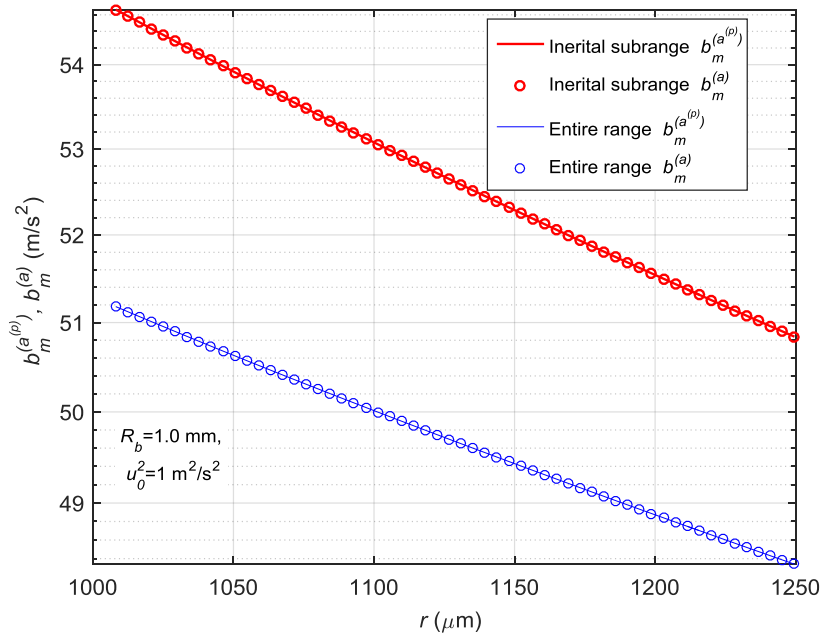

(b)

Figure 6. Comparison of $b_m^{(a)}$ and $b_m^{\left(a^{(p)}\right)}$ results between the inertial subrange and the entire range for $\zeta_{\max}$=1.0 m, $\Delta r = \lambda_K / 5$=4.2μm and u_0^2=1 m^2/s^2.

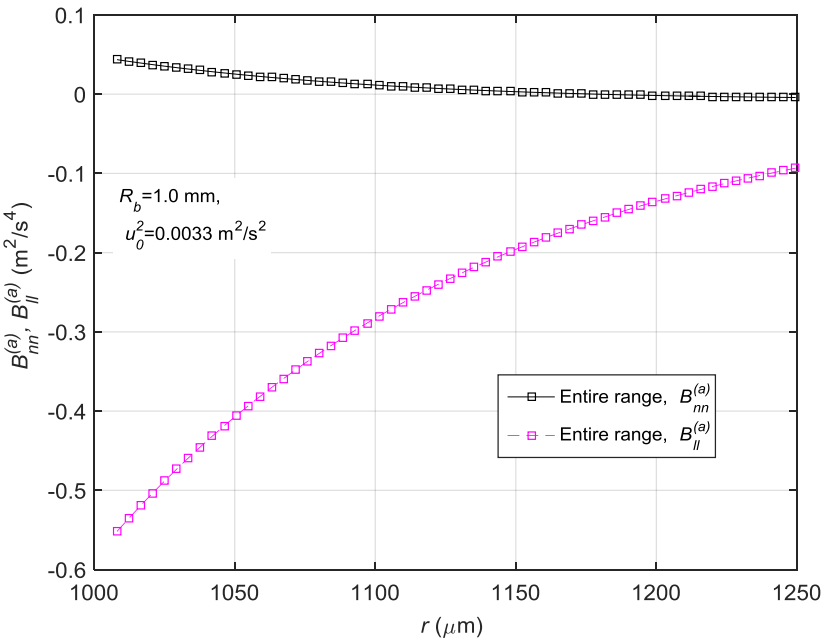

(a)

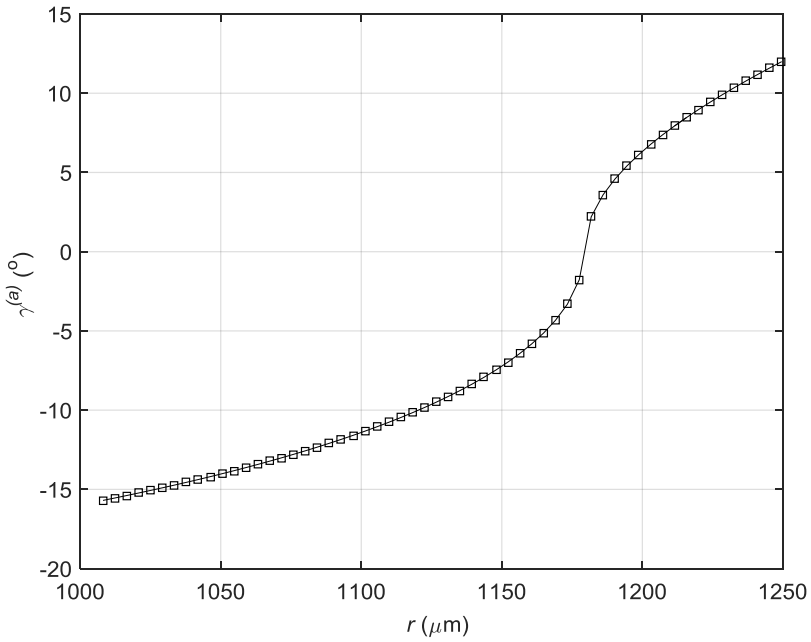

(b)

Figure 7. Numerical results of $B_{nn}^{(a)}, B_{ll}^{(a)}, \gamma^{(a)}$ for the entire range for $\zeta_{\max}$=1.0 m, $\Delta r = \lambda_K / 5$=4.2μm and u_0^2=0.0033 m^2/s^2.

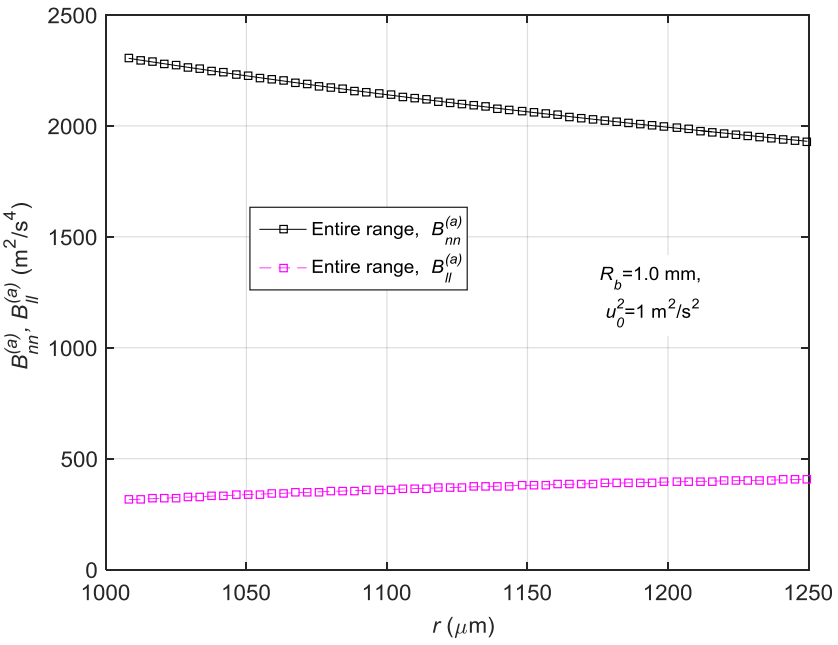

(a)

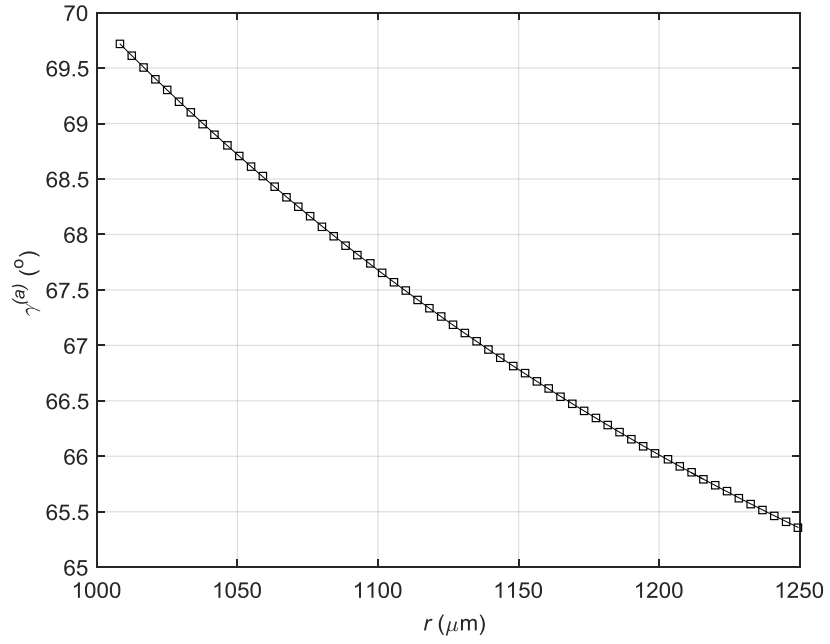

(b)

Figure 8. Numerical results of $B_{nn}^{(a)}, B_{ll}^{(a)}, \gamma^{(a)}$ for the entire range for $\zeta_{\max}$=1.0 m, $\Delta r = \lambda_K / 5$=4.2μm and u_0^2=1 m^2/s^2.

3.3 *Influence of R_b, R_p, ε and u_0^2 on $b_m^{(a)}$ and $\gamma^{(a)}$ for the entire range*

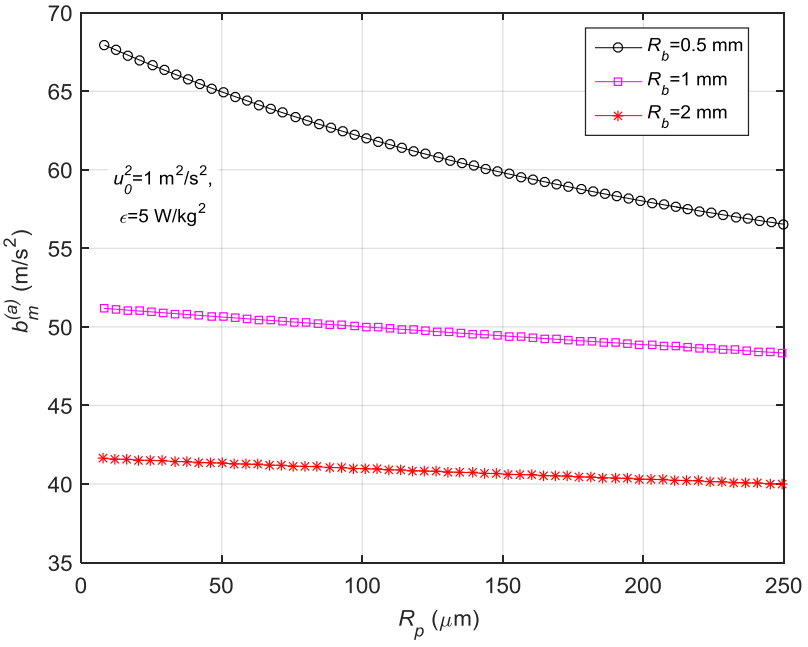

(a)

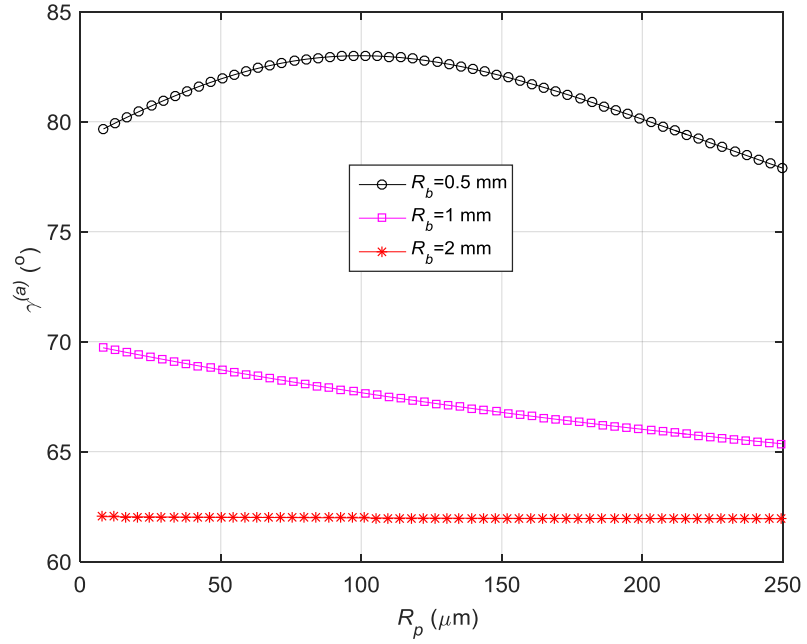

(b)

Figure 9. The entire range case: influence of R_b and R_p on (a) $b_m^{(a)}$ and (b) $\gamma^{(a)}$ for u_0^2=1 m^2/s^2 and ε=5 W/kg .

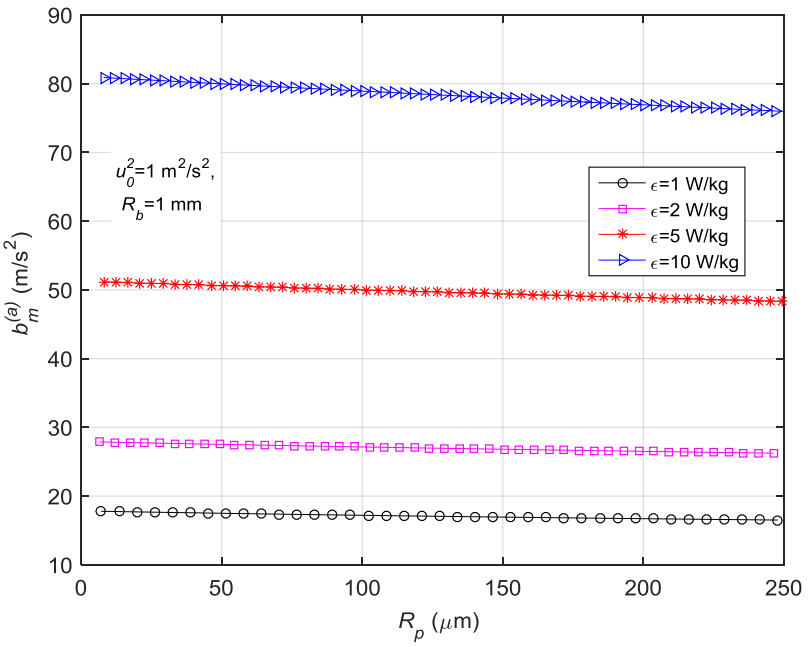

(a)

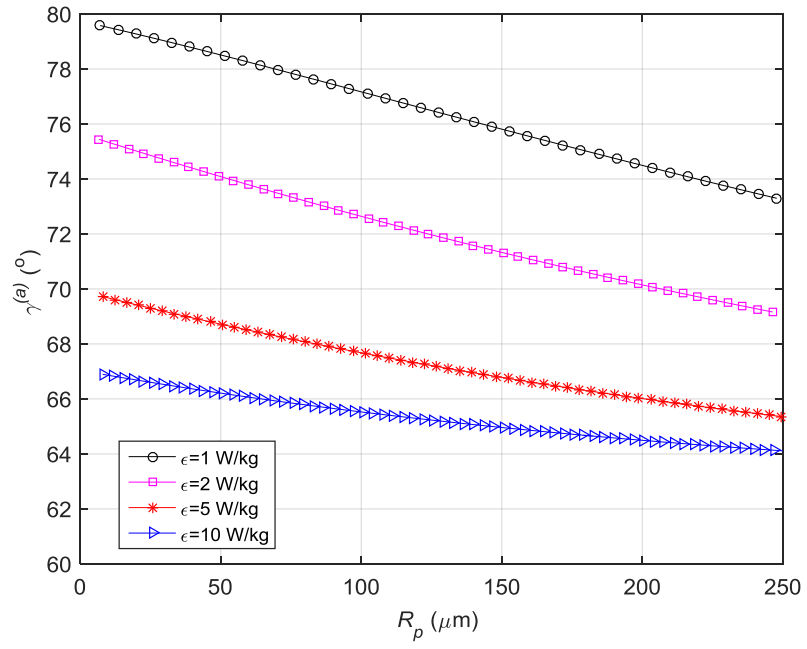

(b)

Figure 10. The entire range case: influence of ε and R_p on (a) $b_m^{(a)}$ and (b) $\gamma^{(a)}$ for u_0^2=1 m^2/s^2 and R_b=1 mm.

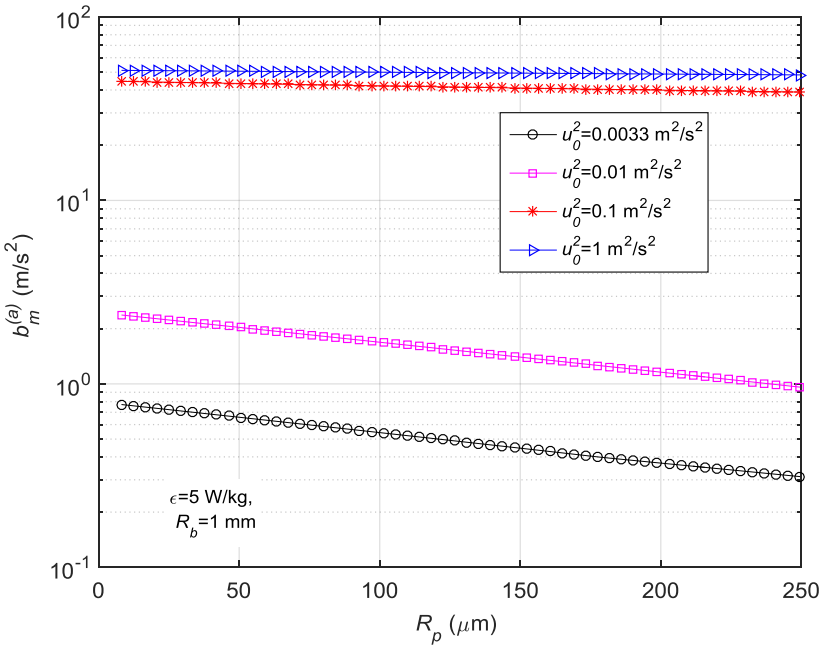

(a)

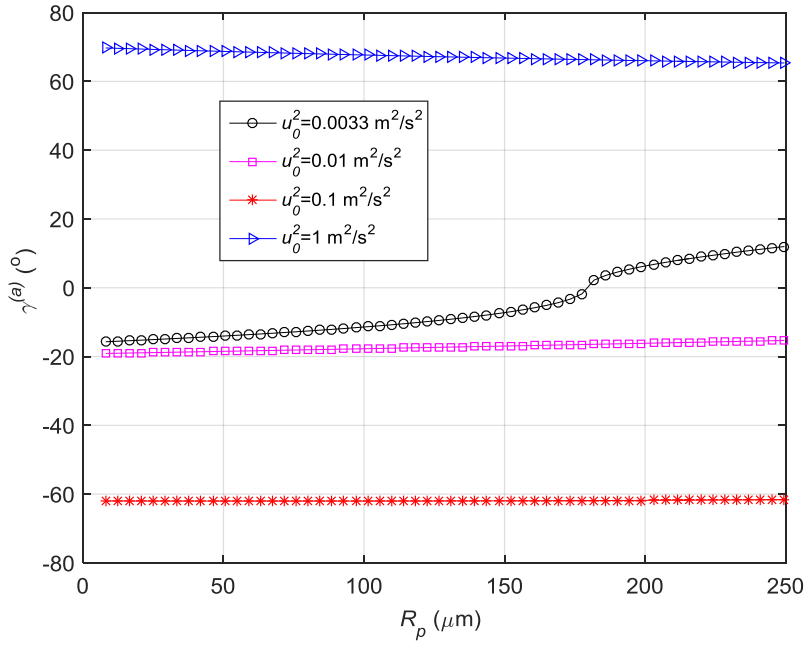

(b)

Figure 11. The entire range case: influence of u_0^2 and R_p on (a) $b_m^{(a)}$ and (b) $\gamma^{(a)}$ for ε=5 W/kg and R_b=1 mm.

Figure 9 shows the influence of R_b and R_p on $b_m^{(a)}$ and $\gamma^{(a)}$ for u_0^2=1 m^2/s^2 and ε=5 W/kg. **Figure 10** presents the influence of ε and R_p on $b_m^{(a)}$ and $\gamma^{(a)}$ for u_0^2=1 m^2/s^2 and R_b=1 mm.

Figure 11 describes the influence of u_0^2 and R_p on $b_m^{(a)}$ and $\gamma^{(a)}$ for ε=5 W/kg and R_b=1 mm. These figures show that $b_m^{(a)}$ reduces with increasing R_p and R_b, and increases with increasing ε and u_0^2. The magnitude of $\gamma^{(a)}$ increases with increasing u_0^2, indicating that the transverse component of turbulence acceleration become more important as increasing the turbulence intensity.

3.4 General discussion

The machine acceleration is determined based on the correlation of the turbulence acceleration due to both the pressure and velocity fields as described by Eqs. (16)-(18), in relation with the longitudinal structure function of velocity fluctuations $D_{ll}^{(V)}$ for the entire range of isotropic turbulence. As shown by Eq. (34), $D_{ll}^{(V)}$ is a function of turbulence intensity (represented by u_0^2) and the Reynolds number Re_λ which is a function of ε and u_0^2 - see Eq. (40). In a mechanical flotation cell, the turbulence intensity $\left(u_0^2\right)$ as well as the dissipation rate of kinetic energy (ε) vary with respect to the position relative to the impeller. Specifically, in the region near the impeller, the values of u_0^2 and ε are high (the transverse component of turbulence acceleration is high) while they are lower in the upper regions of the flotation cell (the transverse component of turbulence acceleration is lower). Therefore, the machine acceleration also varies with the turbulence intensity and the dissipation rate throughout the flotation cell. The information of u_0^2 and ε in the flotation cell can be obtained by using measurement techniques or CFD simulations with an appropriate turbulence model. It is noted that CFD simulation results must be validated by comparison with the experimental data. Therefore, it is highly necessary to develop an accurate measurement technique to determine u_0^2 and ε in the abrasive opaque and multiphase environment in a flotation cell, which is crucial for calculating the machine acceleration.

4. CONCLUSIONS

In this article, we have applied the isotropic turbulence theory in conjunction with the correlation method to examine and extend the concept of machine acceleration. The present model of BP detachment is derived under an assumption that the motion of bubble and particle is the same as that of the liquid particles at their positions, i.e., the density of particles and bubbles is not taken

into account. Our present model of BP detachment (taking into account the viscous effect) and Schulze (1980)'s model (neglecting the viscous effect) yield almost the same results, indicating that the viscous effect is negligible compared to the pressure effect. We have also extended the present model to cover the full range of isotropic turbulence. Since the structure function for the entire range is more complicated than that for the inertial subrange, we have developed a numerical model based on the trapezoidal method and the central-finite difference schemes to calculate the correlation of turbulence acceleration, including its longitudinal and transverse components, and modulus (i.e., the machine acceleration). The numerical model has been successfully verified through the solution for the inertial subrange. Then, the numerical model has been applied for the entire range of isotropic turbulence to investigate the influence of the bubble and particle radii (R_b and R_p), dissipation rate (ε), and mean square of turbulence intensity $\left(u_0^2\right)$ on the correlation of turbulence acceleration. Numerical results show that the machine acceleration reduces with increasing R_p and R_b, and increases with increasing ε and u_0^2. Importantly, the transverse component of turbulence acceleration becomes more important as the turbulence intensity increases. Therefore, both the longitudinal and transverse components of the turbulence acceleration should be considered when quantifying the BP detachment in flotation.

ACKNOWLEDGEMENTS

This research is supported by the Australian Research Council's Project Funding Scheme (Project number DP150100395).

APPENDIX: DETERMINATION THE TRANSVERSE AND LONGITUDINAL COMPONENTS OF $B_{ij}^{\left(a^{(p)}\right)}(r)$ AND $B_{ij}^{\left(a^{(V)}\right)}(r)$

The correlation of the acceleration due to the pressure field $B_{ij}^{\left(a^{(p)}\right)}(r)$ given by Eq. (6) can be re-written as follows:

$$B_{ij}^{\left(a^{(p)}\right)}(r)=\frac{1}{\rho^2}\frac{\partial^2 B^{(p)}}{\partial x_i \partial x_j^*}=-\frac{1}{\rho^2}\frac{\partial^2 B^{(p)}}{\partial r_i \partial r_j}=-\frac{1}{\rho^2}\frac{\partial}{\partial r_i}\left[\frac{r_j}{r}\frac{\partial B^{(p)}}{\partial r}\right] \tag{A.1}$$

$$\therefore B_{ij}^{(a_p)}(\mathbf{r}) = \frac{1}{\rho^2}\left[-\frac{1}{r}\frac{\partial}{\partial r}\left(\frac{1}{r}\frac{\partial B^{(p)}}{\partial r}\right)r_i r_j - \frac{1}{r}\frac{\partial B^{(p)}}{\partial r}\delta_{ij}\right] \tag{A.2}$$

It is noted that $B_{ij}^{(a^{(p)})}(r)$ is the correlation of a random potential vector field. Therefore, the second-order tensor $B_{ij}^{(a_p)}(\mathbf{r})$ in homogeneous isotropic turbulence can be described by

$$B_{ij}^{(a_p)}(\mathbf{r}) = \frac{B_{ll}^{(a_p)} - B_{nn}^{(a_p)}}{r^2} r_i r_j + B_{nn}^{(a_p)}\delta_{ij} \tag{A.3}$$

Making use of Eqs. (A.2) and (A.3) results in the following simplified expressions:

$$B_{nn}^{(a^{(p)})}(r) = -\frac{1}{\rho^2}\frac{1}{r}\frac{\partial B^{(p)}}{\partial r} \tag{A.4}$$

$$B_{ll}^{(a^{(p)})}(r) = -\frac{1}{\rho^2}\frac{\partial^2 B^{(p)}}{\partial r^2} \tag{A.5}$$

The correlation of the acceleration due to the velocity field $B_{ij}^{(a^{(V)})}(r)$ is defined by Eq. (7), where the tensor term can be described as follows:

$$B_{ij}^{(V)}(r) = \frac{B_{ll}^{(V)} - B_{nn}^{(V)}}{r^2} r_i r_j + B_{nn}^{(V)}\delta_{ij} = f r_i r_j + B_{nn}^{(V)}\delta_{ij} \tag{A.6}$$

where the function *f* is defined by Eq. (12). Substituting Eq. (A.6) into Eq. (7) gives

$$B_{ij}^{(a^{(V)})}(r) = \nu^2 D_3^2 f r_i r_j + \nu^2 f_n \delta_{ij} \tag{A.7}$$

where f_n is defined by Eq. (13). Making use of the expression $D_3^2 = \left(\frac{\partial^2}{\partial r^2} + \frac{2}{r}\frac{\partial}{\partial r}\right)\left(\frac{\partial^2}{\partial r^2} + \frac{2}{r}\frac{\partial}{\partial r}\right) = \frac{\partial^4}{\partial r^4} + \frac{4}{r}\frac{\partial^3}{\partial r^3}$, the term $D_3^2\left(f r_i r_j\right)$ in Eq. (A.7) can be expanded as follows:

$$D_3^2\left(fr_ir_j\right)=\left(\frac{\partial^4}{\partial r^4}+\frac{4}{r}\frac{\partial^3}{\partial r^3}\right)\left(fr_ir_j\right)=\frac{\partial^4}{\partial r^4}\left(fr_ir_j\right)+\frac{4}{r}\frac{\partial^3}{\partial r^3}\left(fr_ir_j\right) \tag{A.8}$$

$$\therefore D_3^2\left(fr_ir_j\right)=\left(\frac{4}{r}\frac{\partial^3 f}{\partial r^3}+\frac{\partial^4 f}{\partial r^4}\right)r_ir_j+\left(\frac{24}{r}\frac{\partial f}{\partial r}+36\frac{\partial^2 f}{\partial r^2}+8r\frac{\partial^3 f}{\partial r^3}\right)\delta_{ij} \tag{A.9}$$

Substituting Eq. (A.9) into Eq. (A.7) yields

$$B_{ij}^{\left(a^{(V)}\right)}(r)=\nu^2\left(\frac{4}{r}\frac{\partial^3 f}{\partial r^3}+\frac{\partial^4 f}{\partial r^4}\right)r_ir_j+\nu^2\left(\frac{24}{r}\frac{\partial f}{\partial r}+36\frac{\partial^2 f}{\partial r^2}+8r\frac{\partial^3 f}{\partial r^3}+f_n\right)\delta_{ij} \tag{A.10}$$

The second-order tensor $B_{ij}^{\left(a^{(V)}\right)}(r)$ is described as follows:

$$B_{ij}^{\left(a^{(V)}\right)}(r)=\frac{B_{ll}^{\left(a^{(V)}\right)}-B_{nn}^{\left(a^{(V)}\right)}}{r^2}r_ir_j+B_{nn}^{\left(a^{(V)}\right)}\delta_{ij} \tag{A.11}$$

Combining Eqs. (A.10) and (A.11), we obtain the following predictions:

$$B_{nn}^{\left(a^{(V)}\right)}=\nu^2\left(\frac{24}{r}\frac{\partial f}{\partial r}+36\frac{\partial^2 f}{\partial r^2}+8r\frac{\partial^3 f}{\partial r^3}+f_n\right) \tag{A.12}$$

$$B_{ll}^{\left(a^{(V)}\right)}=\nu^2\left(\frac{24}{r}\frac{\partial f}{\partial r}+36\frac{\partial^2 f}{\partial r^2}+12r\frac{\partial^3 f}{\partial r^3}+r^2\frac{\partial^4 f}{\partial r^4}+f_n\right) \tag{A.13}$$

NOMENCLATURE

Small alphabet letters

a_i	Flow acceleration in the $i-$direction
$a_i^{(p)}$	A potential vector field defined as $a_i^{(p)}=-\frac{1}{\rho}\frac{\partial p}{\partial x_i}$
$a_i^{(V)}$	A solenoidal vector field defined as $a_i^{(V)}=\nu\Delta V$

b_m Machine acceleration

d_b Bubble diameter

d_p Particle diameter

f A function defined as $f = \dfrac{B_{ll}^{(V)} - B_{nn}^{(V)}}{r^2}$

f_m A function defined as $f_m = D_3 B_{nn}^{(V)}$

f_n A function defined as $f_n = D_3^2 \left(B_{nn}^{(V)} \right)$

g Gravitational acceleration

p Flow pressure

r The sum of bubble and particle radii

t Time

u_0^2 Mean square intensity of turbulence

Capitalised alphabet letters

$B_{ll}^{(*)}$ Longitudinal component of a correlation function

$B_{nn}^{(*)}$ Transverse component of a correlation function

$B_{ij}^{(a)}$ Correlation function of fluctuating acceleration of two liquid particles

$B_{ij}^{\left(a^{(p)}\right)}$ Correlation function of fluctuating acceleration of two liquid particles due to pressure

$B_{ij}^{\left(a^{(V)}\right)}$ Correlation function of fluctuating acceleration of two liquid particles

$B^{(p)}$ Correlation function of pressure at two positions

$B_{ij}^{(V)}$ Correlation function of fluctuating velocity of two liquid particles

C A constant, $C \approx 2.0$

D_3 $D_3 = \Delta^* = \Delta = \Delta_r = \left(\dfrac{\partial^2}{\partial r^2} + \dfrac{2}{r} \dfrac{\partial}{\partial r} \right)$

D_3^2 $D_3^2 = \Delta\Delta^* = \Delta^2 = \dfrac{\partial^4}{\partial r^4} + \dfrac{4}{r} \dfrac{\partial^3}{\partial r^3}$

$D_{ll}^{(*)}$ Longitudinal component of a structure function

$D_{nn}^{(*)}$ Transverse component of a structure function

$D^{(p)}$ A structure function of flow pressure

$D^{(V)}$ A structure function of flow velocity

$\mathbf{F}_{B_{bp}^{(a)}}$ A detachment force associated with $B_{bp}^{(a)}$

$\mathbf{F}_{B_{bpll}^{(a)}}$ The longitudinal component of $\mathbf{F}_{B_{bp}^{(a)}}$

$\mathbf{F}_{B_{bpnn}^{(a)}}$ The transverse component of $\mathbf{F}_{B_{bp}^{(a)}}$

N The total number of grid points in the computational domain

Ne The relative error norm defined by (44)

R_b Bubble radius

R_p Particle radius

Re_λ Reynolds number defined as $\mathrm{Re}_\lambda = \left(\frac{15 u_0^4}{\varepsilon \nu} \right)^{1/2}$

$\mathbf{V}$ Flow velocity

V_i Flow velocity in the $i-$direction

Greek letters

γ The angle between the total force $\mathbf{F}_{B_{bp}^{(a)}}$ and the BP center-line

ε Turbulence dissipation rate

λ_K Kolmogorov length scale

Λ Macro-turbulence length scale

Δr Grid size

ζ A coordinate variable in Eq. (14)

$\zeta_{\max}$ The maximum value of ζ

μ Dynamic viscosity of a fluid

ν Kinematic viscosity of a fluid

ρ Fluid density

ρ_b Bubble density

ρ_p Particle density

τ_K Kolmogorov time scale

REFERENCES

Alipchenkov, V.M., Zaichik, L.I., Particle clustering in isotropic turbulent flow. Fluid Dynamics, 2003, **38(3)**, 417-432.

Goel, S., Jameson, G.J., Detachment of particles from bubbles in an agitated vessel. Minerals Engineering, 2012, **36**, 324-330.

Jameson, G.J., New directions in flotation machine design. Minerals Engineering, 2010, **23(11-13)**, 835-841.

Jameson, G.J., Nguyen, A.V., Ata, S., 2007. The flotation of fine and coarse particles, In *Froth Flotation: A Century of Innovation*, eds. Fuerstenau, M.C., Jameson, G.J., Yoon, R.-H. SME, Denver, CO, USA, pp. 329-351.

Nguyen, A.V., An-Vo, D.-A., Tran-Cong, T., Evans, G.M., A review of stochastic description of the turbulence effect on bubble-particle interactions in flotation. International Journal of Mineral Processing, 2016, **156**, 75-86.

Nguyen, A.V., Schulze, H.J., *Colloidal Science of Flotation*. 2004, Marcel Dekker, New York.

Panchev, S., Haar, D.t., *Random Functions and Turbulence*. 1971, Pergamon Press, Oxford.

Schulze, H.J., New theoretical and experimental investigations on stability of bubble/particle aggregates in flotation: a theory on the upper particle size of floatability. International Journal of Mineral Processing, 1977, **4(3)**, 241-259.

Schulze, H.J., Dimensionless number and approximate calculation of the upper particle size of floatability in flotation machines. International Journal of Mineral Processing, 1982, **9(4)**, 321-328.

Wang, G., Evans, G.M., Jameson, G.J., Bubble–particle detachment in a turbulent vortex I: Experimental. Minerals Engineering, 2016a, **92**, 196-207.

Wang, G., Evans, G.M., Jameson, G.J., Bubble-particle detachment in a turbulent vortex II—Computational methods. Minerals Engineering, 2017, **102**, 58-67.

Wang, G., Nguyen, A.V., Mitra, S., Joshi, J., Jameson, G.J., Evans, G.M., A review of the mechanisms and models of bubble-particle detachment in froth flotation. Separation and Purification Technology, 2016b, **170**, 155-172.

Zaichik, L., Alipchenkov, V.M., Sinaiski, E.G., *Particles in Turbulent Flows*. 2008, Wiley-VCH, Weinheim.